

## Frictional Moisture Convergence in a Composite Life Cycle of the Madden–Julian Oscillation

ERIC D. MALONEY AND DENNIS L. HARTMANN

*Department of Atmospheric Sciences, University of Washington, Seattle, Washington*

(Manuscript received 24 June 1997, in final form 7 October 1997)

### ABSTRACT

A composite life cycle of the Madden–Julian oscillation (MJO) is constructed using an index based on the first two EOFs of the bandpass-filtered (20–80 days) 850-mb zonal wind averaged from 5°N to 5°S every 2.5° around the equator. Precipitation, 1000-mb convergence, 850-mb wind, and 200-mb wind are composited for the period 1979–95. Water vapor integrated from the surface to 300 mb is composited for the period 1988–92.

Frictional moisture convergence at the equator is shown to play an important role in the life cycle of the Madden–Julian oscillation (MJO). Regions of boundary layer convergence foster growth of positive water vapor anomalies to the east of convection. This convergence coincides with 850-mb easterly wind anomalies, as is consistent with Kelvin wave dynamics. Drying of the atmosphere occurs rapidly after the passage of convection with the onset of 850-mb westerly perturbations. Possible mechanisms for this drying include boundary layer divergence and subsidence or horizontal advection from the west or extratropics associated with Rossby wave circulations. Frictional convergence in front of convection helps to slowly moisten the atmosphere to a state that is again favorable for convection. This moistening may set the timescale for the reinitiation of convection in the Indian and west Pacific Oceans after strong drying and provides a mechanism for slow eastward propagation. A significant correlation exists between surface convergence and column water vapor anomalies in the west Pacific and Indian Oceans. Weaker correlations exist between 850-mb convergence and water vapor anomalies. Over the west Pacific, surface convergence leads positive water vapor anomalies, while 850-mb convergence lags positive water vapor anomalies.

Northern Hemisphere summer (May–October) composites show that the phases of the MJO coincide with “active” and “break” periods of the Indian summer monsoon at intraseasonal timescales. The northward propagation of precipitation across India during the summer monsoon is associated with northward and westward movement of Rossby wave features trailing the main center of equatorial convection associated with the MJO.

### 1. Introduction

Much has been published concerning the Madden–Julian oscillation (MJO) since it was first discovered by Madden and Julian (1971, 1972) in rawinsonde and sea level pressure data from the tropical oceans. The MJO is now understood to be a dominant mode of variability in the tropical circulation that has characteristic periods of 30–60 days (Madden and Julian 1994). Ultimately, a complete understanding will probably involve the interaction among convection, wave dynamics, boundary layer circulations, and moisture. This paper seeks to further that understanding by constructing a composite life cycle of the MJO using wind, convergence, water vapor, and precipitation fields.

Recent work suggests the importance of interactions among the large-scale wave, the boundary layer, and convection in determining the mechanisms that give rise

to the MJO. Frictional convergence in the boundary layer east of the main convective area has been shown to be important in the evolution and eastward propagation of the MJO in several recent modeling studies (Wang and Rui 1990; Salby et al. 1994; Seager and Zebiak 1994; Wang and Li 1994). Observational evidence has also shown that the convective anomaly associated with the MJO is tied to convergence processes in the boundary layer. Hendon and Salby (1994) showed this by compositing the 1000-mb divergence field in relation to outgoing longwave radiation (OLR). Convection is fostered in areas of boundary layer convergence, while boundary layer divergence suppresses convection. A recent study by Jones and Weare (1996) using the International Satellite Cloud Climatology Project and European Centre for Medium-Range Weather Forecasts (ECMWF) analyses has also shown that the maximum low-level moisture convergence occurs to the east of the main convective area. Surface convergence provides an upward flux of moisture in the boundary layer by increasing the low-level equivalent potential temperature through moistening (e.g., Seager and Zebiak 1994).

---

*Corresponding author address:* Eric Maloney, Department of Atmospheric Sciences, University of Washington, Box 351640, Seattle, WA 98195–1640.  
E-mail: maloney@atmos.washington.edu

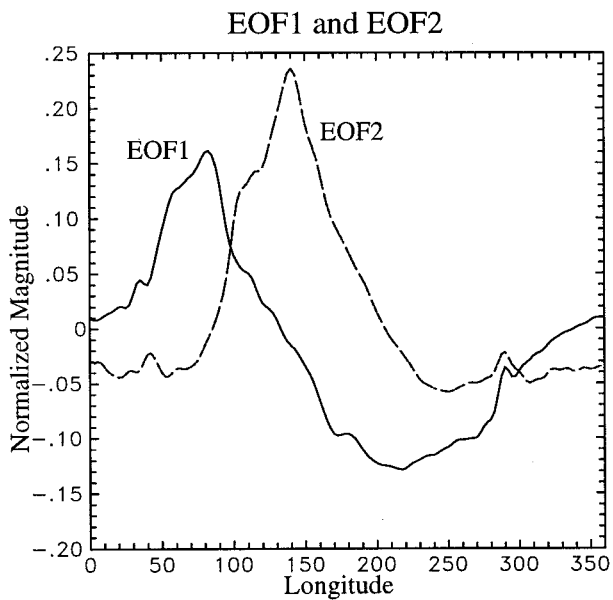


FIG. 1. EOF 1 (solid) and EOF 2 (dashed) of 850-mb zonal wind as a function of longitude. Magnitudes were normalized in the computation of the EOFs.

Geostrophic zonal wind dynamics, as in classical equatorial Kelvin wave theory, requires that inviscid lower-tropospheric easterly wind perturbations be accompanied by a surface pressure trough at the equator, whereas inviscid lower tropospheric westerlies should be accompanied by a pressure maximum (Matsuno 1966). Therefore, friction will foster convergence into the equatorial pressure trough below 850-mb easterlies. Since the growing convective area associated with the MJO over the Indian Ocean is accompanied by 850-mb easterlies to the east over the west Pacific (Knutson and Weickmann 1987; Hendon and Salby 1994), convection will be supported by boundary layer convergence to the east and suppressed to the west, where 850-mb westerly perturbations and surface divergence are found. Rossby wave generation in the Indian Ocean in the presence of convective heating may also dry the atmosphere to the west of convection through subsidence or horizontal advection from the west or extratropics (Gill 1980). Some previous studies have suggested that the atmosphere goes through a period of preconditioning before being able to sustain convection associated with the MJO (Hendon and Liebmann 1990; Bladé and Hartmann 1993; Hu and Randall 1994). The humidity profile at a fixed point in the lower troposphere moistens slowly and then dries quickly as the convection passes and westerly winds ensue (Bladé and Hartmann 1993). These studies reason that a period of buildup of moist static energy is required for the atmosphere to recover from the previous cycle of convection, which had the effect of stabilizing and drying the atmosphere. In the present study we speculate that a period of buildup of moisture is required over the Indian and west Pacific

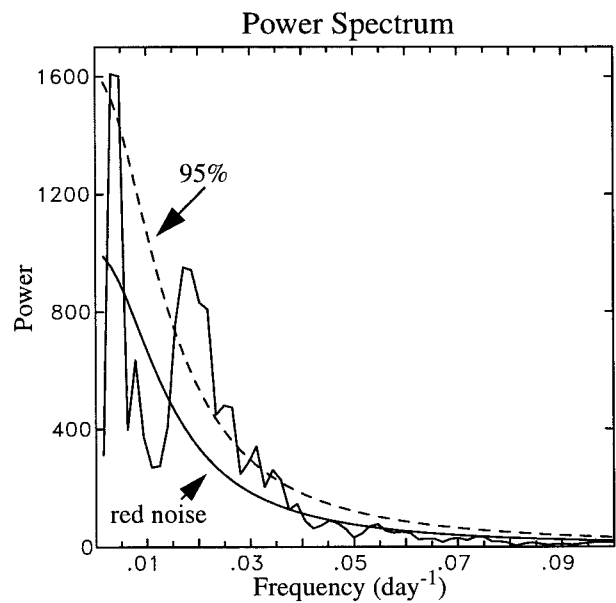


FIG. 2. Power spectrum of the index obtained by projecting the first two EOFs onto the unfiltered equatorial time series of 850-mb zonal wind for 1979–95. The red noise spectrum is displayed along with the a priori 95% confidence limit (dotted).

Oceans before significant convection can occur, and that this may in fact set the timescale for the jump in convection from the Indian Ocean to the west Pacific Ocean. Frictional surface convergence may be a key player in this preconditioning of the atmosphere.

Hendon and Salby (1994, hereafter referred to as HS) composited 200- and 850-mb wind, microwave sounding unit (MSU) temperature, OLR, 1000-mb wind, 850-mb divergence, and 1000-mb divergence anomalies. The observed composites are similar to the typical picture derived from modeling studies of a coupled equatorial Rossby–Kelvin wave (e.g., Wang and Li 1994). The HS composites show that maximum convergence at 1000 mb precedes inviscid convergence at 850 mb, which is consistent with the ideas examined in modeling studies. Divergence at 1000 mb lags to the west of convection and may contribute to its demise when the convective area is engulfed by 850-mb westerly perturbations.

The present study takes a similar strategy as HS in creating a composite MJO life cycle as a function of nine phases. In this study, however, the compositing technique, the choice of fields composited, and the method of filtering are significantly different from HS. First, we use 850-mb zonal wind as a compositing basis instead of OLR. Whereas in HS a regression analysis on OLR is used, this paper creates an index for compositing based on the first two (EOFs) of the 850-mb equatorial zonal wind and then selects events based on this index. Details of the technique will be described in subsequent sections. Second, like HS, this paper composites the fields of 200- and 850-mb wind, along with 1000-mb convergence. In addition to the fields consid-

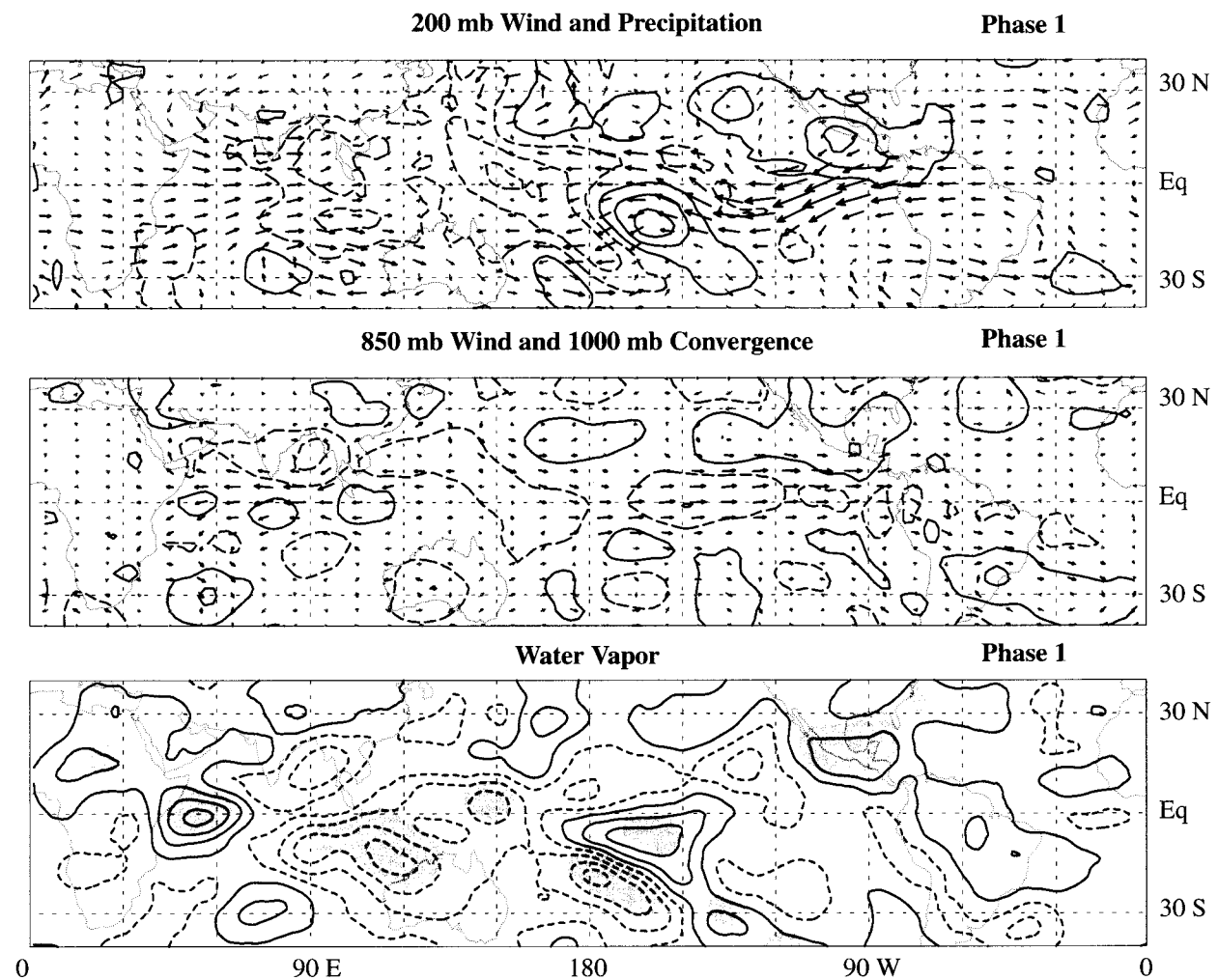


FIG. 3. The top two panels are phase 1 composites of bandpassed 200- and 850-mb wind anomalies, MSU precipitation anomalies (without annual cycle), and the bandpassed 1000-mb convergence anomaly field for the period 1979–95 (all seasons). Significant vectors are shown in black while others are shown in gray. The third panel is a composite of NVAP water vapor anomalies (without annual cycle) integrated to 300 mb, displayed for the years 1988–92. Maximum wind vectors are  $6.1 \text{ m s}^{-1}$  and  $2.8 \text{ m s}^{-1}$  for 200 mb and 850 mb, respectively. Precipitation contours are at intervals of  $0.6 \text{ mm day}^{-1}$  starting at  $0.3 \text{ mm day}^{-1}$ . Convergences are at intervals of  $2 \times 10^{-7} \text{ s}^{-1}$  starting at  $1 \times 10^{-7} \text{ s}^{-1}$ . Water vapor anomalies are at intervals of  $0.8 \text{ mm}$  starting at  $0.4 \text{ mm}$ . Regions significant at the 90% level are shaded. Convergence contours are solid and divergences are dashed. Negative contours are dashed for precipitation and water vapor.

ered by HS, precipitable water anomalies are composited, along with MSU precipitation in place of OLR. Composites of precipitable water give supporting evidence that regions of boundary layer convergence actually lead to increased water column in areas undergoing surface convergence. The MSU precipitation data give a better indication of the location of heating than OLR, at least over the oceans. Thus, the MSU precipitation field is able to give a more detailed picture of fine structure associated with convective areas. A third significant departure is that HS zonally filtered all fields to zonal wavenumbers 1–3, whereas this study uses no zonal filtering. The composites in HS consequently cannot resolve the separate amplification of convection over the Indian and west Pacific Oceans (Weickmann and

Khalsa 1990; Salby and Hendon 1994), a fact that is duly noted in HS. As will be seen later, the composites created here are able to resolve the Indian Ocean convective center and the west Pacific convective center and detail the transition between the two regions.

The seasonal dependence of the MJO has been examined in some detail in previous studies [a good review can be found in Madden and Julian (1994)], and an examination of the Northern Hemisphere summer composites in this study proves to be somewhat enlightening. Particularly interesting is the role of the MJO in the regulation of the Indian summer monsoon. Previous studies have examined this aspect of the MJO and have shown that “break” periods of the Indian monsoon seem to occur on intraseasonal timescales, with strong indi-

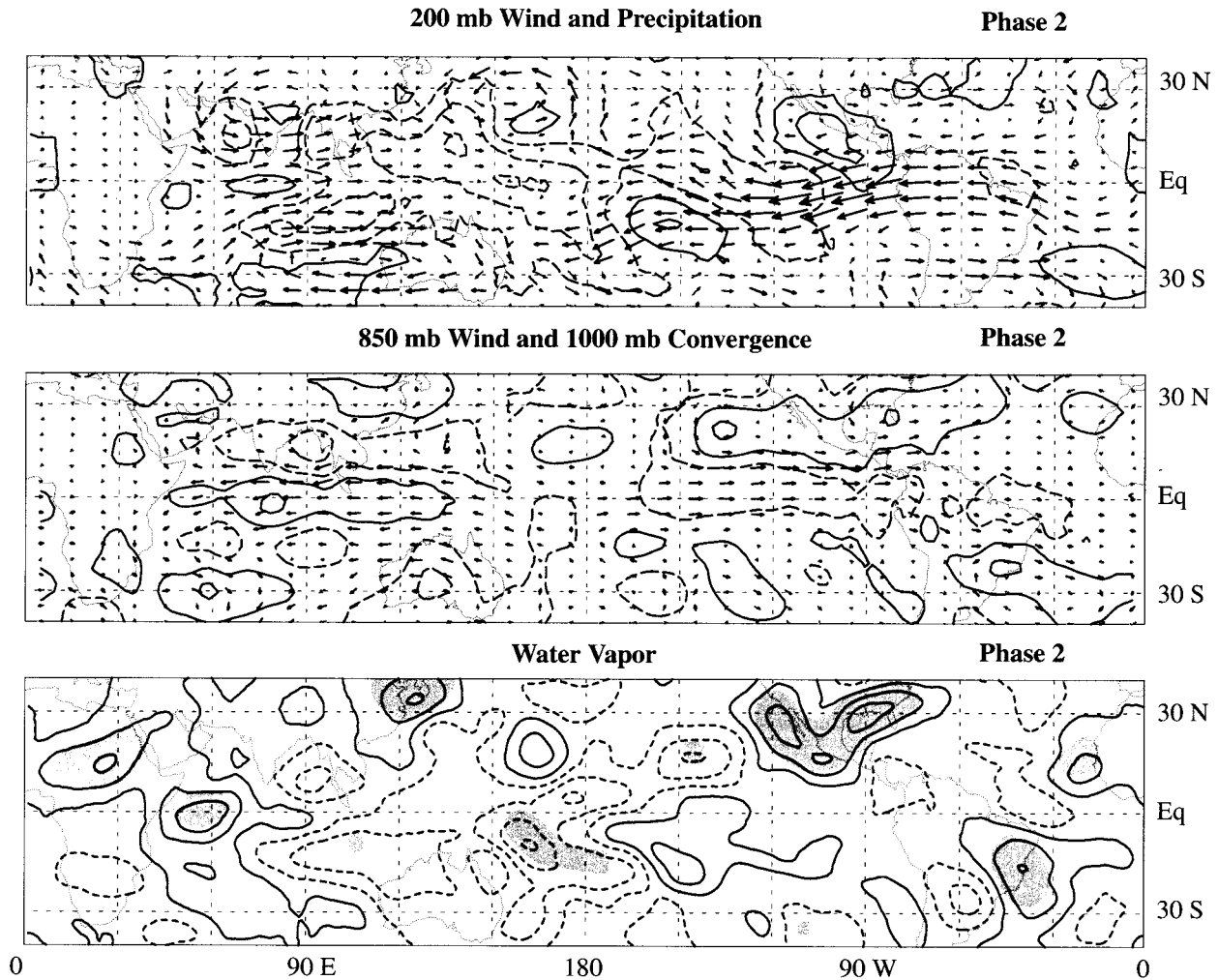


FIG. 4. Same as Fig. 3 but for phase 2.

cations of being phase-locked to MJO events (e.g., Hartmann and Michelsen 1989; Madden and Julian 1994). Creating a composite view of the NH summer case proves to be very interesting in this respect in that break and “active” periods of the monsoon can be directly traced to the phase of the MJO being examined in the composites. High spatial resolution shows that Rossby wave structure is responsible for northward propagating precipitation areas.

Section 2 describes the data products used and section 3 describes the compositing technique. Section 4 will present the composites created for all seasons of the year, while section 5 will look at the Northern Hemisphere summer. Conclusions will be presented in section 6.

## 2. Data

The National Centers for Environmental Prediction–National Center for Atmospheric Research (NCEP–NCAR) reanalysis data (Kalnay et al. 1996) were used

for the 200-, 850-, and 1000-mb wind fields. Convergences were derived using these wind fields. Pentad (5-day mean) averages were used from 1979–95 in a gridded  $2.5^\circ \times 2.5^\circ$  format. Operational ECMWF analyses were originally used in the study, but then replaced by the NCEP–NCAR reanalysis product when it became available. The NCEP–NCAR data for the entire 1979–95 period were derived from the same model and data assimilation scheme. Our results do not significantly differ for the two datasets. In this study the wind convergence at 1000 mb plays an important role. Over the oceans the surface winds are largely generated by the model dynamics and boundary layer scheme, and not by direct observations, so our conclusions are subject to the assumption that the model produces realistic surface wind convergence. Surface meridional convergence anomalies at  $165^\circ\text{E}$  and the equator from NCEP–NCAR and the Tropical Atmosphere Ocean buoy array were compared for the years 1988–95 using the compositing technique described in section 3. Similar anomalies were

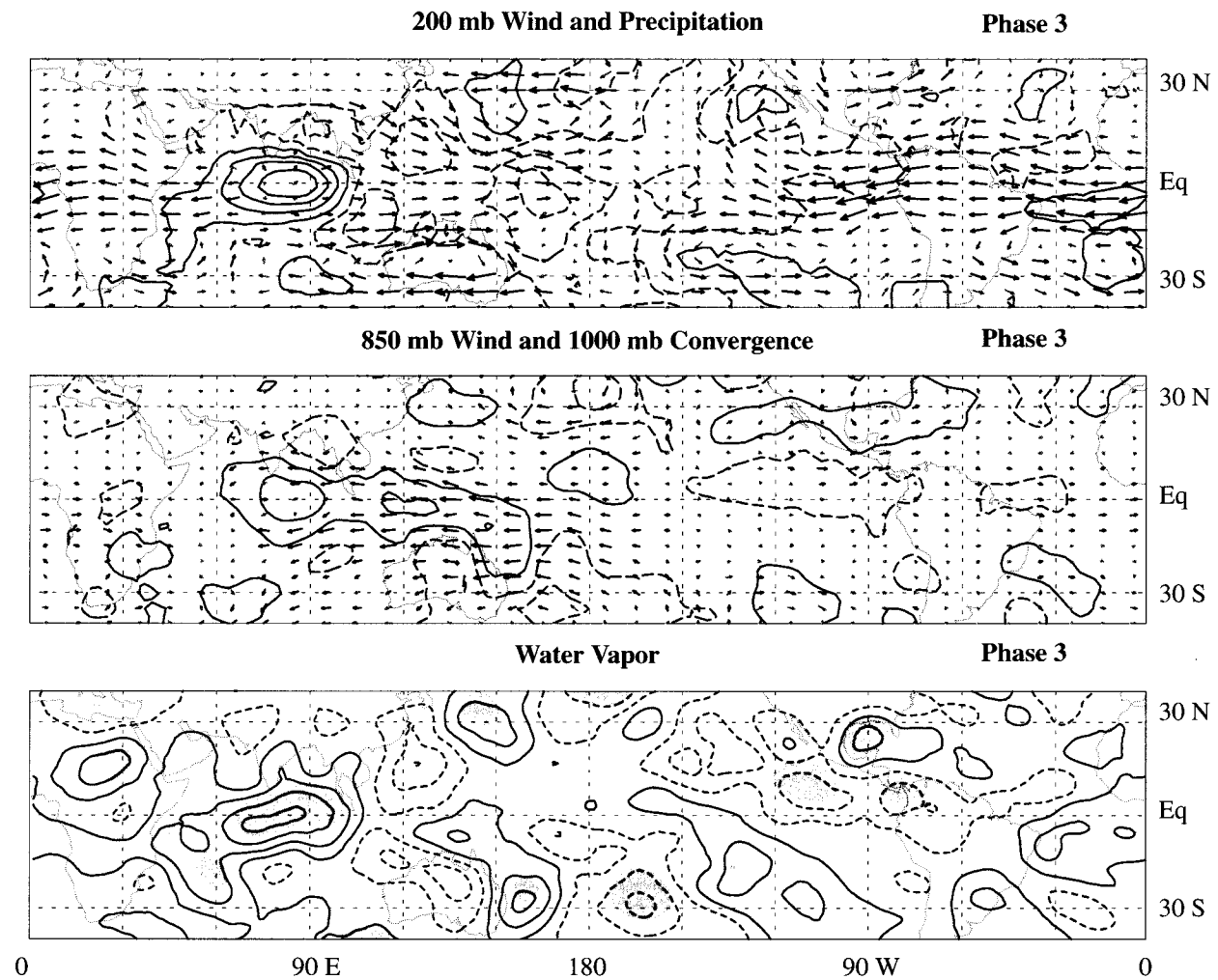


FIG. 5. Same as Fig. 3 but for phase 3.

seen in both datasets (not shown), although the sample size was too small to produce statistically significant results.

MSU precipitation data were used in pentad form for the years 1979–95. The precipitation dataset is derived by using channel 1 of the microwave sounding unit, which is sensitive to emission by cloud water and rainwater in the lowest few kilometers of the atmosphere (Spencer 1993). The MSU precipitation product is only able to detect precipitation over the ocean, which is adequate for this study, since ocean surface dominates the region of interest. The reliability of MSU precipitation over the Maritime Continent is a question, but the OLR signal does not indicate any strong convective signals over island areas that do not exist in the MSU precipitation data. The Advanced Very High Resolution Radiometer National Oceanic and Atmospheric Administration (NOAA) OLR product (Gruber and Krueger 1984) was used to corroborate signals in MSU precip-

itation in certain key regions, and proved useful in examining signals around the Indian subcontinent.

The NASA Water Vapor Project (NVAP) precipitable water data (Randel et al. 1996) were available from 1988–92 in pentad form. The NVAP product is a merged product of three different datasets: radiosonde, Special Sensor Microwave/Imager, and Television Infrared Observational Satellite operational vertical sounder. The merged product gives water vapor values for three different levels: surface–700 mb, 700–500 mb, and 500–300 mb.

### 3. Compositing technique

The index used for compositing was constructed using the 20–80-day bandpass-filtered 850-mb zonal wind field. The 850-mb zonal wind was averaged from 5°N to 5°S every 2.5° around the equator. EOF analysis was then done on the resulting equatorially averaged zonal

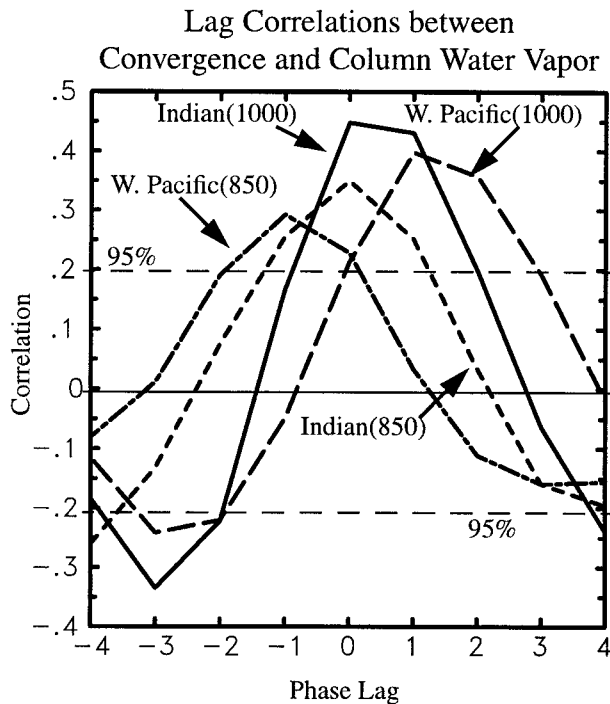


FIG. 6. Plot of lag correlations between 850- and 1000-mb convergence and column water vapor anomalies in the Indian and west Pacific Oceans as a function of the lag in phases for 1979–95 (all seasons). A positive phase lag means convergence leads water vapor. Indian Ocean correlations are averaged over an area from  $5^{\circ}\text{N}$  to  $5^{\circ}\text{S}$  and  $65^{\circ}$  to  $85^{\circ}\text{E}$  (solid, 1000 mb; short dash, 850 mb). West Pacific correlations are averaged over an area from  $5^{\circ}\text{N}$  to  $5^{\circ}\text{S}$  and  $130^{\circ}$  to  $150^{\circ}\text{E}$  (long dash, 1000 mb; dotted dash, 850 mb). The dashed horizontal lines represent the limits at which correlations are significantly different from zero at the 95% level at 1000 mb for the west Pacific Ocean.

wind field for the entire 1241 pentad record (1979–95). EOF 1 and EOF 2 are displayed in Fig. 1. EOF 1 explains 32% of the total bandpass-filtered variance, while EOF 2 explains 22%. EOFs 3 and 4 explained 10% and 7%. Using the criterion developed by North et al. (1982), the first two EOFs are significantly different from the rest. Principal component analysis by projection of the first two EOFs onto the filtered 850-mb zonal wind field shows that the principal component for EOF 1 peaks in magnitude an average of two to three pentads before the principal component for EOF 2.

EOF 1 and EOF 2 appear to form a propagating signal in the zonal wind. EOF 1 in its positive polarity appears to show westerlies at lower levels over the Indian Ocean changing over to easterlies over the Pacific Ocean at roughly  $130^{\circ}\text{E}$ . Peaking 2–3 pentads later, EOF 2 corresponds to the strong low-level westerly winds that accompany many MJO events over the western and central Pacific Oceans (e.g., Lau et al. 1989). Further progression with time reveals that the EOFs nicely depict the cycle of 850-mb wind perturbations that accompany MJO events that have been detailed in prior observa-

tional work (e.g., Madden and Julian 1972; Knutson and Weickmann 1987; Hendon and Salby 1994).

An index was constructed in the following manner, where  $t$  is the time in pentads:

$$\text{Index}(t) = \text{PC1}(t) + [\text{PC2}(t + 2) + \text{PC2}(t + 3)]/2. \quad (1)$$

The index is a linear combination of the principal components (PCs) of EOF 1 and EOF 2. Since the principal component of EOF 2 peaks an average of 2–3 pentads after the principal component of EOF 1, contributions from the principal component of EOF 2 both 2 and 3 pentads later are added to the principal component of EOF 1 in order to form the index. The results are insensitive to reasonable variations in the time at which PC 2 is taken into account. Since the PCs are proportional to the amplitude explained, no weighting between PC 1 and PC 2 other than this is required. The selection of events is not sensitive to this weighting. The time at which the index is at a maximum is when a region of maximum convergence of the 850-mb zonal wind anomalies is centered at about  $130^{\circ}\text{E}$ .

To test whether or not the index indeed captures the essence of the zonal wind signal associated with the MJO, the first two EOFs were projected onto the *unfiltered* 850-mb zonal wind time series averaged over  $5^{\circ}\text{S}$  to  $5^{\circ}\text{N}$ . The index above was then reconstructed using these unfiltered principal components and the power spectrum was computed. The results of the spectral analysis are shown in Fig. 2. Two features are readily apparent. A large peak is associated with the annual cycle and, most importantly, a second peak prominently stands above the background spectrum at intraseasonal periods of roughly 30–80 days. The intraseasonal peak is significantly different from the red noise spectrum at the 95% level. This zonal wind index thus captures the nature of the MJO, even when projected onto unfiltered data.

Once the index was constructed, phases were assigned. The time variation of the index is that of an oscillating pattern much like a sinusoidally varying function. Key events were determined by choosing events that had peak amplitudes greater than one standard deviation away from zero. Periods in which the index did not have succeeding positive and negative anomalies were ignored, but as it turns out, these periods would have been filtered out by the selection process regardless, because the magnitudes were small during these times. Criteria such as choosing events with maximum peak to trough amplitude and maximum trough amplitude were also tried, and the results were found to be insensitive to the exact criterion used. As a result of this selection criterion, 81 events were isolated during the period 1979–95 for all seasons. Once the events were isolated, each event was broken into nine different phases for compositing. Phase 5 was designated the time in each event at which the index had maximum peak amplitude. Phase 1 and phase 9 were given to the times

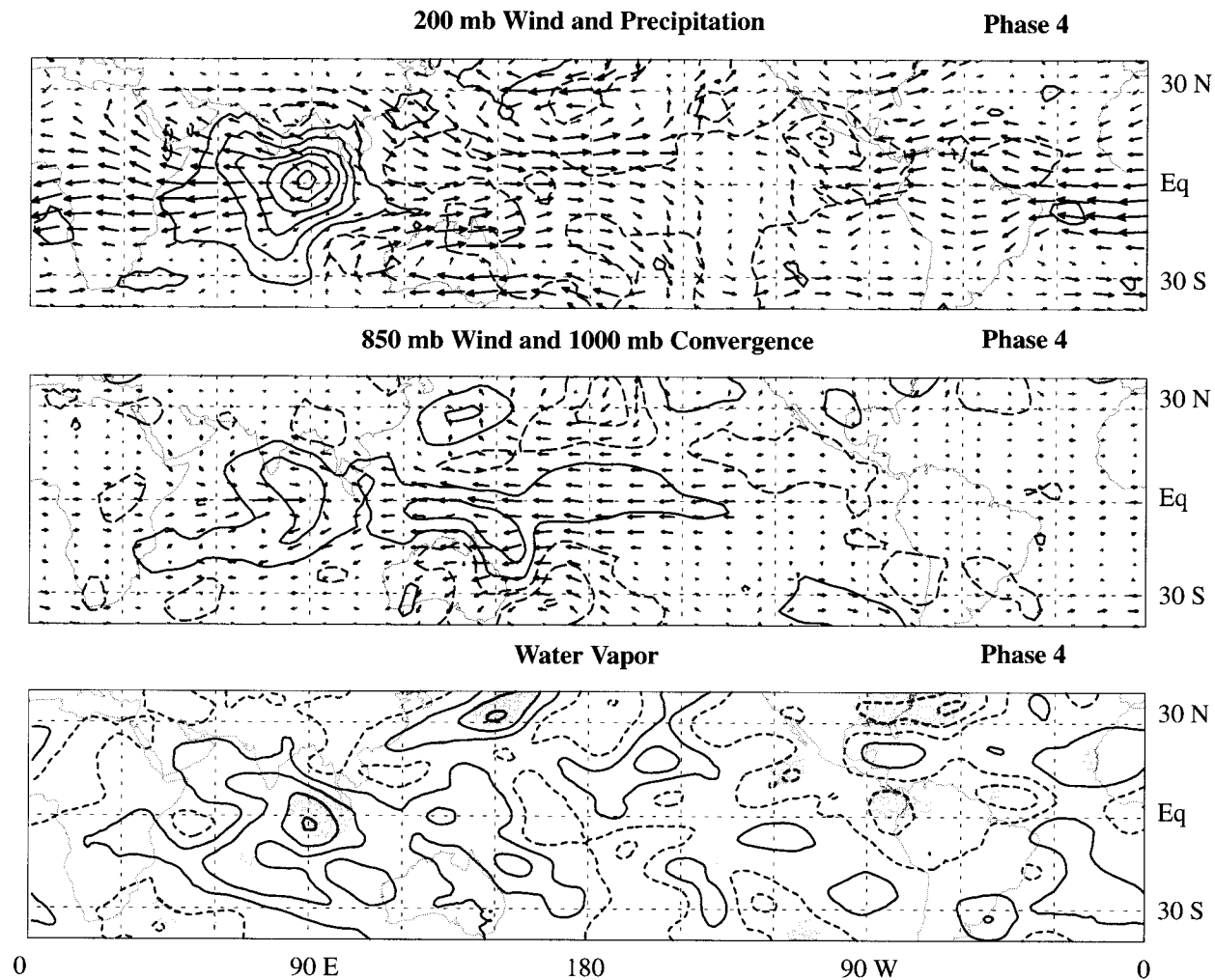


FIG. 7. Same as Fig. 3, but for phase 4.

in each event with largest trough amplitude before and after phase 5, respectively. Phases 3 and 7 were given to the zero increasing and zero decreasing points in each event, and the other phases were placed equidistant in

time between phases 1, 3, 5, 7, and 9. The 81 events were then averaged together to produce a composite event.

Water vapor values were available for only the years

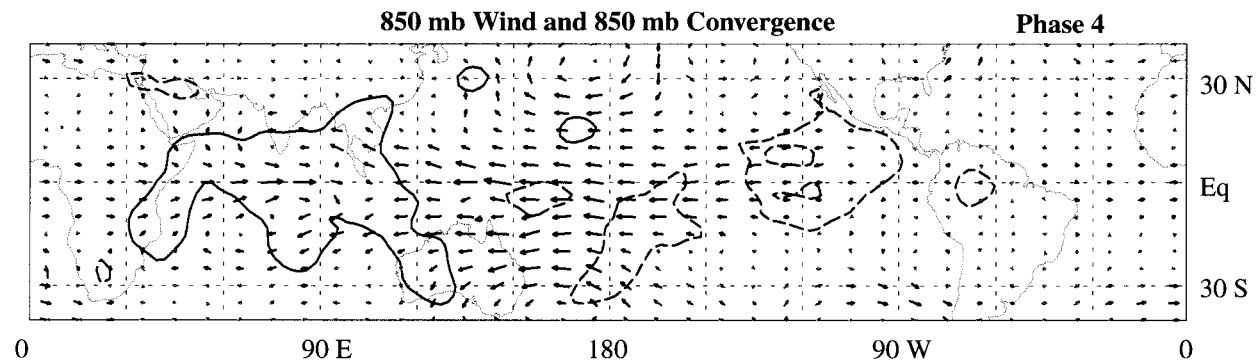


FIG. 8. Wind anomaly at 850 mb and 850-mb convergence anomaly field for phase 4. Contour interval is  $2 \times 10^{-7} \text{ s}^{-1}$  starting at  $1 \times 10^{-7} \text{ s}^{-1}$ . Wind vectors are of same magnitude as Fig 7.

1988–92, so the number of events included in the water vapor composites is only 28. Compositing the fields other than water vapor for the years 1988–92 showed the same features as for the longer period of 1979–95, so we feel it is justified to display the water vapor composites alongside the composites for the other variables that were determined from the entire 1979–95 record.

#### 4. Composites

Figures 3–14 (see later sections) detail the evolution of a composite cycle of the MJO. All seasons are included. Wind fields were bandpass filtered to 20–80 days and convergences were derived from these filtered wind fields. The annual cycle was removed from the precipitation and water vapor fields. Winds at 200 mb are displayed along with MSU precipitation for all nine phases. Vectors that are significantly greater than zero at the 90% level are plotted in black. The significance of wind vectors was determined by comparing the magnitude of the vector wind anomalies to a null hypothesis of zero. Winds at 850 mb are displayed along with the 1000-mb convergence field. Water vapor anomalies are displayed with the 90% significance levels shaded. Since the patterns in the water vapor field show no significant dependence on the particular level examined, we show the anomalies of column integrals from the surface to 300 mb. In the Indian and west Pacific Oceans at the lowest levels, the moisture anomalies in our composites correspond to equivalent potential temperature variations of 2°–3°C.

##### *a. Phase 1*

Figure 3 shows the situation at phase 1 of the composite cycle. At this time the precipitation anomaly over the Indian Ocean is weakly negative. Westerly 200-mb wind anomalies extend across this region with easterlies at 850 mb. Pockets of surface convergence can be seen near the equator over the Indian Ocean in association with the 850-mb easterly winds, a theme that will be repeated in the composite pictures for other phases. A positive water vapor anomaly appears over the western Indian Ocean at about 50°E near the westernmost convergence center at 1000 mb. A small anomaly appears in the precipitation record coincident with the water vapor record from 1988 to 1992 (not shown). The precipitation anomaly is not significant, whereas the water vapor anomaly is. The development of a strong positive water vapor anomaly without a strong signal in precipitation over the western Indian Ocean is intriguing. It is notable that this same feature will appear in phase 9. The timing of this feature in phases 8 and 9 seems to correspond to the onset of easterly 850-mb wind anomalies in this region.

Farther to the east, negative precipitation anomalies and negative water vapor anomalies are occurring from the central Indian Ocean near 70°E eastward to the date

line. The remnants of the previous cycle of convection can be seen just to the east of the date line at about 10°S. Significant water vapor anomalies match up nicely with this feature. Westerly anomalies at 850 mb and strong 200-mb easterly wind anomalies occur from the date line eastward to past 60°W. Another intriguing feature that is also seen in phase 9 is the positive precipitation and water vapor anomaly to the south of Mexico and Central America extending northwestward from 90°W. This feature is most prominent in the Northern Hemisphere summer (not shown). This precipitation is coincident with cyclonic shear of the zonal wind associated with the westerly wind anomaly near the equator at 850 mb. It seems possible that the MJO may play some role in regulating tropical cyclone activity in this region of the eastern Pacific Ocean. However, further research is needed to confirm this relationship.

##### *b. Phase 2*

In phase 2, weak positive anomalies in precipitation are present over the equatorial Indian Ocean at the African coast and at about 80°E (Fig. 4). The eastern edge of this developing precipitation area is where the main convective area for the Indian Ocean will develop during subsequent phases. The water vapor anomaly has expanded slightly toward the east. Both the precipitation and water vapor anomalies are growing in a region of increasing 1000-mb convergence that is expanding eastward with the 850-mb easterly wind perturbations. Negative water vapor anomalies over the western Pacific and the Maritime Continent (90°–150°E) have begun to weaken along the equator in the area coincident with the surface convergence. We hypothesize that surface convergence plays the necessary role of eroding negative water vapor anomalies over the west Pacific thereby creating an environment favorable for convection. Upper-tropospheric wind perturbations are westerly over the equator from 60° to 150°E and are associated with cyclones in the 200-mb wind field at about 25°N and 25°S, a picture consistent with HS.

To the east, a weak area of convection can still be found near 150°W and 15°S. Precipitation and water vapor anomalies are still enhanced along the Mexican and Central American coasts associated with summertime convection. The 1000-mb convergence field continues to show positive anomalies over this area also. Rather strong easterly 200-mb wind anomalies are occurring along and just to the south of the equator from 150° to 30°W.

##### *c. Phase 3*

In phase 3 rainfall begins to blossom in the eastern Indian Ocean at about 80°E (Fig. 5). This convection is accompanied by a strong water vapor anomaly. The convection is accompanied by surface convergence, which extends eastward of the convection with the 850-

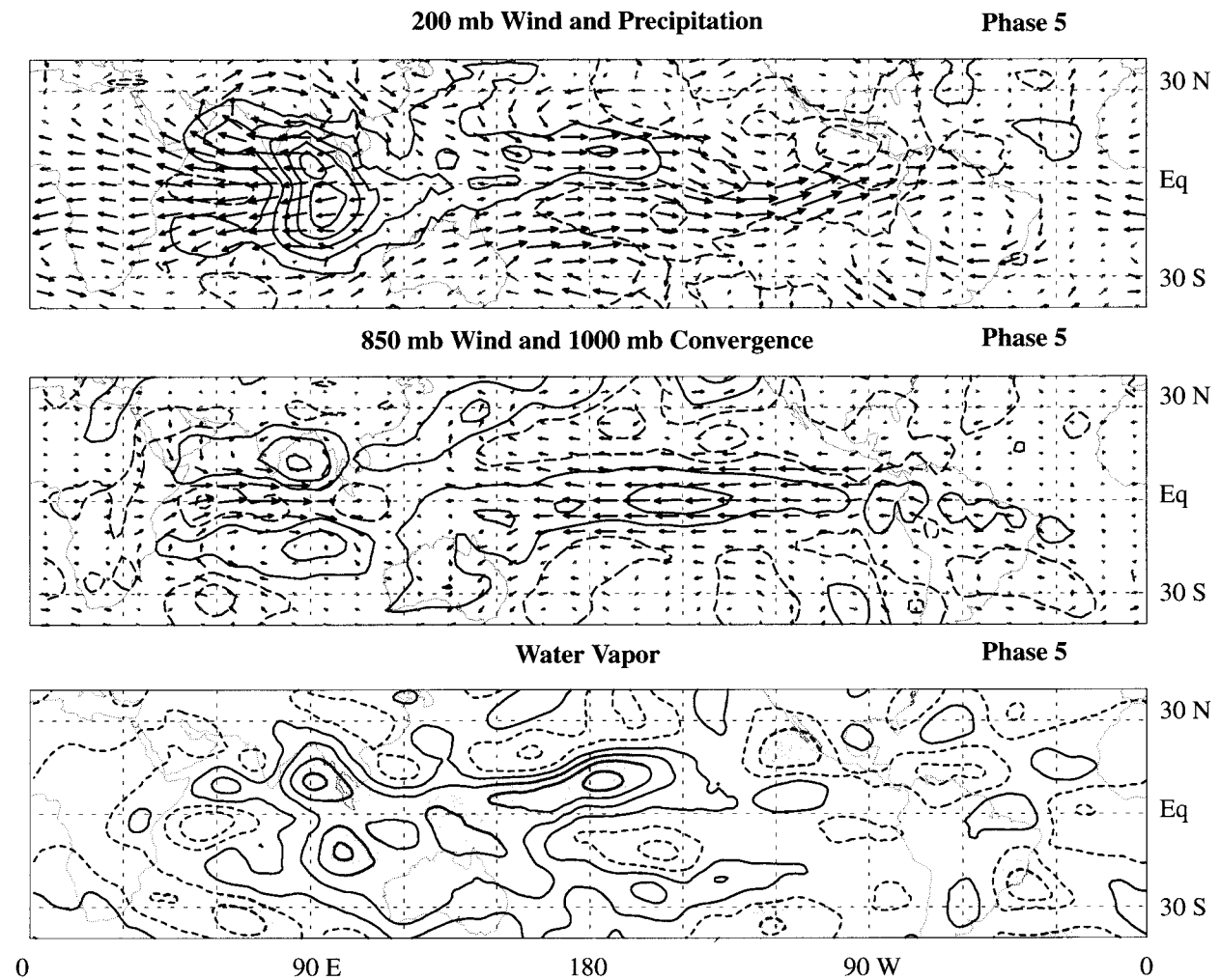


FIG. 9. Same as Fig. 3 but for phase 5.

mb easterlies that extend to about 160°E. The water vapor field shows that the negative anomalies over the equatorial west Pacific have been eliminated and some positive anomalies are developing near 150°E, which is consistent with persistent surface convergence in these areas. Positive anomalies in the water vapor field generally precede positive anomalies in the precipitation field in the western and central Pacific Ocean. This suggests that the atmosphere in this region needs to be preconditioned before convection is able to occur there. This idea is similar to the idea proposed by Hendon and Liebmann (1990), Bladé and Hartmann (1993), and Hu and Randall (1994) that the atmosphere requires a period of buildup of moist static energy before convective events can be maintained. In the present paper, we see that surface convergence acts to increase the precipitable water in the west Pacific and thus increase the moist static energy of that region. The drying of the atmosphere after passage of the previous convective event is counteracted in part by the moistening of the atmosphere by surface convergence below the 850-mb east-

erly wind perturbations. In the Indian Ocean also, a buildup of moisture anomalies serves as a precursor to the actual convective event. As was seen in phase 1, a strong buildup of anomalies in the water vapor field occurs before the strong onset of convection in the Indian Ocean near 80°E, although the precursor event in the Indian Ocean is not collocated with the main convective development.

Figure 6 shows lag correlations between convergence at 1000 and 850 mb and column-integrated water vapor anomalies for the Indian and west Pacific Oceans. Convergence at 1000 mb leads positive vapor anomalies by zero to one phases over the Indian Ocean and one to two phases over the west Pacific Ocean. Positive correlations on the order of 0.4–0.45 that are significantly different from zero at the 95% level are found in both regions. Convergence at 850 mb lags positive vapor anomalies by one phase over the west Pacific Ocean with no phase lag over the Indian Ocean. Correlations between 850-mb convergence and vapor anomalies are lower (0.3–0.35) than for 1000-mb convergence. These

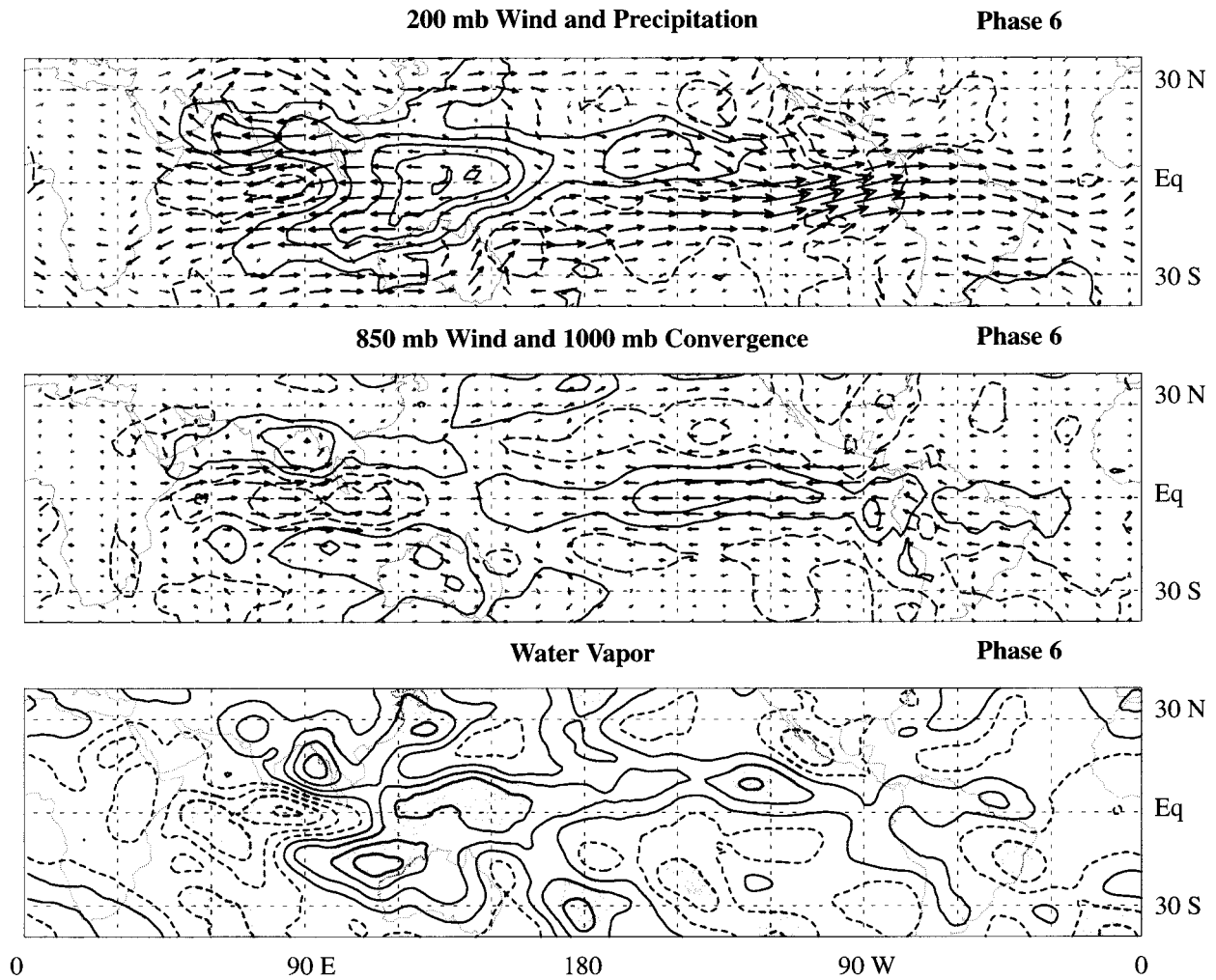


FIG. 10. Same as Fig. 3 but for phase 6.

correlations provide evidence that surface convergence and water vapor anomalies are indeed linked and that convergence at 850 mb is not crucial for the development of water vapor anomalies.

#### d. Phase 4

Phase 4 shows the convection over the Indian Ocean at its peak (Fig. 7). The center of convection has moved very little since phase 3, indicating that this convective center is virtually growing in place over the eastern Indian Ocean between  $80^{\circ}$  and  $85^{\circ}$ E along the equator. Hendon and Salby (1994) note that the same stationary feature in convection would have been obtained in their composites had they not filtered all fields to zonal wavenumbers 1–3. Positive water vapor anomalies have now taken hold eastward from this area to about  $150^{\circ}$ E along the equator, and a tongue of surface convergence now extends to about  $135^{\circ}$ W in the company of 850-mb easterly perturba-

tions. These easterlies are flanked to the north and south by anticyclones evident in the 850-mb wind field and cyclones at 200 mb. The precipitation anomaly to the south of Central America has reversed. Negative precipitation anomalies and anticyclonic shear of the 850-mb zonal wind will continue to develop in this area during subsequent phases. The beginning of cyclones in the 850-mb wind field can be seen to the immediate northwest and southwest of the main convective region, along with a broader anticyclone pair in the 200-mb wind field. These features are consistent with Rossby wave propagation away from the main convective area. Circulation patterns in the Indian Ocean appear to be most interesting during Northern Hemisphere summer, particularly north of the equator. These will be examined in more detail in section 5.

Westerly perturbations at 850 mb are apparent from the Indian Ocean convection westward. A dry water vapor anomaly is beginning to grow near  $50^{\circ}$ E. A couple of mechanisms may explain the appearance of this

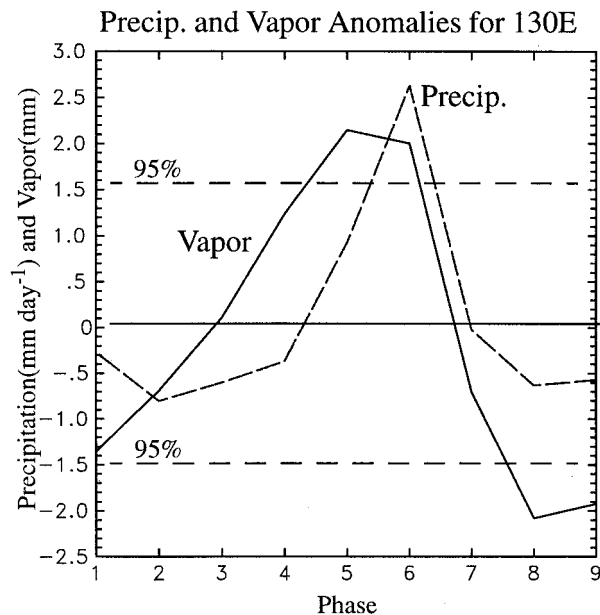


FIG. 11. Precipitation anomalies and water vapor anomalies for the years 1988–92 (all seasons) as a function of phase for a  $5^\circ \times 5^\circ$  box centered at the equator and  $130^\circ\text{E}$ : precipitation (dashed) and vapor (solid). The dotted horizontal lines are the limits at which the water vapor signal is significantly different from zero at the 95% level.

anomaly. One possibility is that surface divergence (barely detectable by the first contour level over the western Indian Ocean) due to an equatorial pressure maximum dries the lower atmosphere. Second, subsidence or horizontal advection from the west or extratropics associated with Rossby wave circulations may dry the air (Gill 1980). Subsequent composites will show that these westerlies will form a wedge of dry anomalies along the equator that will act to suppress convection in areas affected by it. Winds at 200 mb are out of phase with those at 850 mb and display easterly anomalies.

Returning to the idea of surface convergence, the 850-mb convergence and wind fields are plotted for phase 4 in Fig. 8. Although at 1000 mb a tongue of convergence extends across the equatorial Pacific to about  $130^\circ\text{W}$ , no such tongue is found at 850 mb. This implies that it is the surface convergence that must be causing the moisture increase to the east of the main convective area and not the effect of inviscid convergence. Inviscid convergence is prominent in the region at which 850-mb easterly and westerly zonal wind anomalies converge along the equator, but not toward the east. Convergence fields are generally weaker for the 850-mb field than for the 1000-mb field.

#### e. Phase 5

Interesting things occur in the Indian and western Pacific Oceans during phase 5 (Fig. 9). Convection at the equator in the Indian Ocean is no longer being sup-

ported by surface convergence and is consequently beginning to move off the equator accompanied by cyclonic (anticyclonic) circulations at 850 mb (200 mb) to the north and south of the equator at about  $80^\circ\text{E}$ . As discussed earlier, these low-level cyclones and upper-level anticyclones are characteristic of the Rossby wave response seen with the MJO. A split in the anomaly pattern is rather well shown in the 1000-mb convergence field and water vapor field. Bands of surface convergence at about  $15^\circ\text{N}$  and  $15^\circ\text{S}$  flank the equatorial divergence over the Indian Ocean. Westerly 850-mb wind perturbations have split the convective center into two separate convective centers on either side of the equator. This same structure has been reproduced in several recent modeling studies (Wang and Rui 1990; Salby et al. 1994; Seager and Zebiak 1994; Wang and Li 1994).

To the east of the convective region, strong water vapor anomalies are now present in the west Pacific, along with growing precipitation anomalies. It appears that the atmosphere is becoming sufficiently moistened for convection to be favored in the west Pacific. A strong tongue of positive water vapor anomalies also extends past the date line at about  $5^\circ\text{--}10^\circ\text{N}$ . Weak positive precipitation anomalies are becoming apparent in this tongue of moisture anomalies. This precipitation structure resembles an intertropical convergence zone (ITCZ) and is forming in the transition zone between positive and negative surface convergence anomalies. Thus, the link between this development and surface convergence is inconclusive. However, the link between surface convergence and vapor anomalies in the western Pacific is robust. The surface convergence signal now extends along the equator to South America in association with the 850-mb easterly wind perturbations. Weak water vapor anomalies are also present in the vicinity of South America. Negative water vapor anomalies and suppressed precipitation are present just to the south and west of Central America.

#### f. Phase 6

Phase 6 shows a rather impressive structure in the precipitation field (Fig. 10). The main equatorial convective anomaly has made the transition from the Indian Ocean to the west Pacific around  $130^\circ\text{E}$ . Bands of precipitation at about  $15^\circ\text{N}$  and  $15^\circ\text{S}$  extending across the northern and southern Indian Ocean are associated with Rossby waves evident in both the 1000-mb convergence field and the water vapor anomaly field. Strong anticyclonic circulations at 200 mb in association with these features are readily apparent. At the equator in the Indian Ocean strong 850-mb westerly anomalies and surface divergence are present with a strong tongue of anomalously low precipitation and water vapor values extending across the Indian Ocean. Rapid drying of the atmosphere occurs in association with these westerly anomalies. Possible mechanisms for this drying were discussed in section 4d.

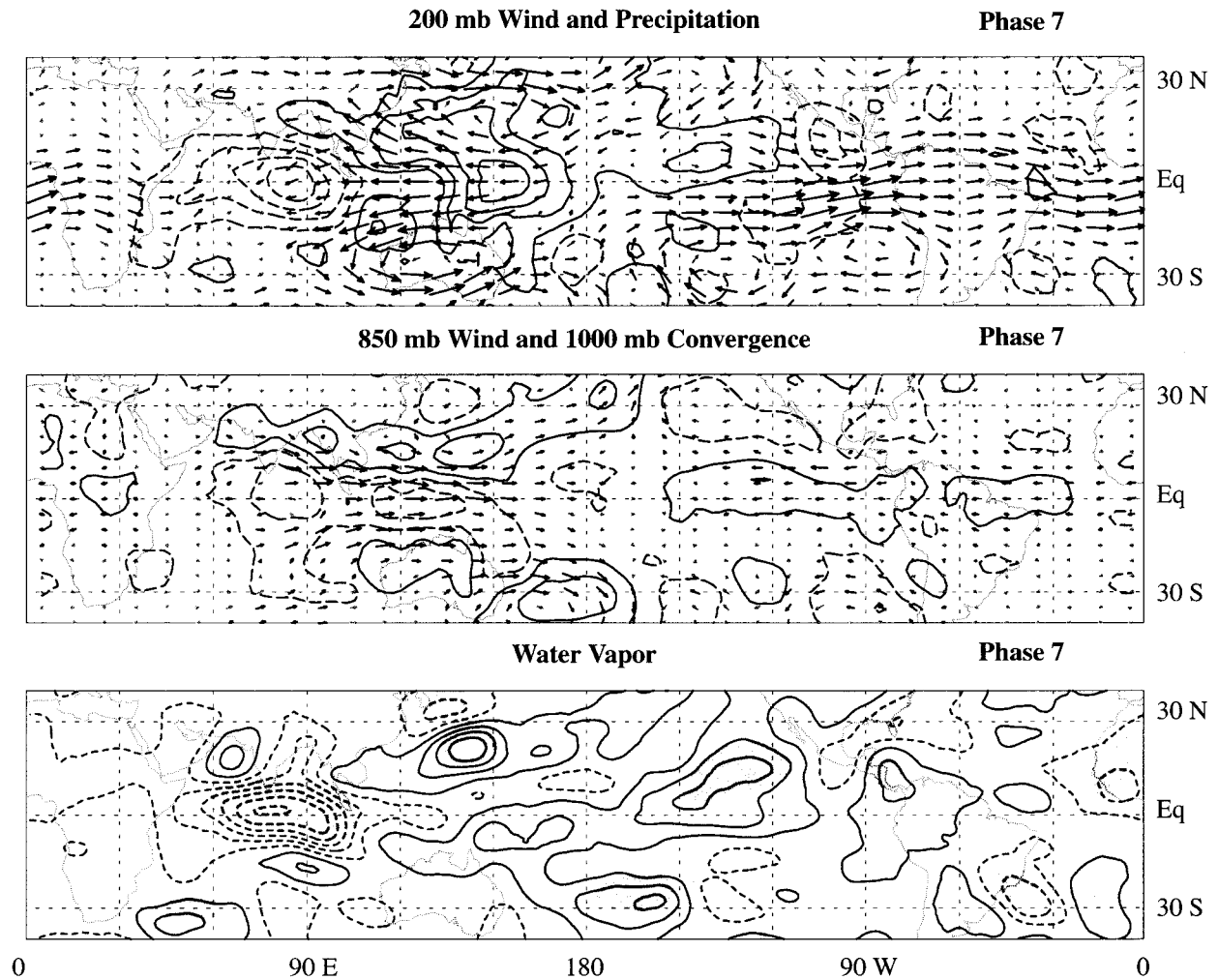


FIG. 12. Same as Fig. 3 but for phase 7.

The main convective area is at a node in the surface convergence at  $130^{\circ}\text{E}$ , with strong convergence to the east toward South America. Strong positive water vapor anomalies are occurring along and to the north of this convergence. An ITCZ signature in the precipitation extends out to  $120^{\circ}\text{W}$  at about  $5^{\circ}\text{--}10^{\circ}\text{N}$ . A similar ITCZ structure was detected by Bantzer and Wallace (1996). Strong 850-mb easterly perturbations and very strong 200-mb westerly perturbations straddle the equator just to the south of the ITCZ.

The phase relationship between the precipitation signal and the water vapor signal over the west Pacific is interesting. To show this relationship, a  $5^{\circ} \times 5^{\circ}$  box centered at the equator and  $130^{\circ}\text{E}$  was chosen and water vapor anomalies and precipitation anomalies were plotted as a function of phase (Fig 11). Results from this region were typical of the western equatorial Pacific in general. Water vapor anomalies are increasing over this region after phase 1. The precipitation anomalies only start to increase significantly after phase 4. Positive wa-

ter vapor anomalies are reached at phase 3 preceding the onset of positive precipitation anomalies at phase 5. The vapor anomaly peaks at phase 5 or 6, whereas the precipitation anomaly peaks at phase 6. After they peak, both fields decline rapidly. This suggests again that the atmosphere needs to be slowly preconditioned before convection can begin in earnest, and that the passage of the maximum in convection and large-scale wave structure quickly dries the atmosphere. Surface convergence associated with the 850-mb easterly perturbations of a Kelvin wave helps to slowly moisten the atmosphere, and rapid drying accompanies the strong 850-mb westerly anomalies of the Rossby and Kelvin wave features after the passage of convection.

#### g. Phase 7

At phase 7 the convective center has shifted to  $155^{\circ}\text{E}$  with a bull's-eye of suppressed precipitation and humidity over the Indian Ocean accompanied by 1000-mb

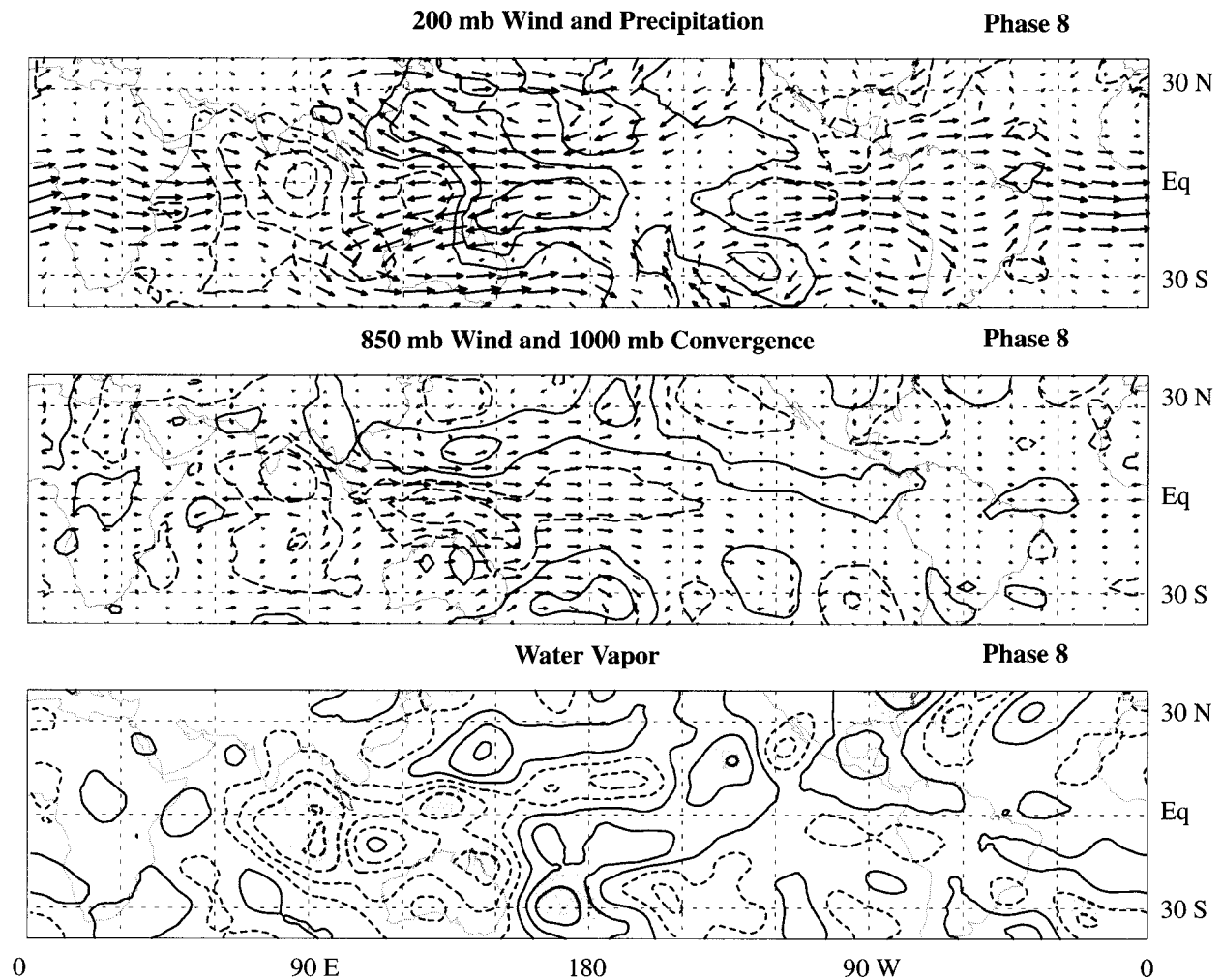


FIG. 13. Same as Fig. 3 but for phase 8.

divergence (Fig. 12). Westerly 850-mb wind anomalies are continuing to drive into the convective area with precipitation areas to the north and south of the equator at about 120°E flanking the strong westerlies at lower levels. Strong anticyclones at 200 mb accompany these features in association with Rossby waves at 130°E. A strong dry anomaly is located over the Indian Ocean to the west of the main convective area with some moist anomalies stretching eastward from the main convective area to about 110°W with additional pockets over South America. Surface convergence has weakened over the east Pacific Ocean along the equator and strong moist anomalies in the water vapor field are beginning to decay and become disjointed. An ITCZ still extends out to about 120°W. The main convective area is in a region of surface divergence now as the equatorial Kelvin wave begins to propagate away from the central Pacific, and 850-mb westerly wind anomalies overtake the convective area.

*h. Phase 8*

The convective area over the central Pacific at 170°E has weakened and the water vapor anomaly has started to become diffuse over the central and east Pacific (Fig. 13). Evidence for a positive ITCZ anomaly still remains just to the north of the equator. The dry anomaly over the Indian Ocean has expanded into the west Pacific Ocean to about 150°E, and it is this anomaly that must be eroded in order for convection to be reestablished in the west Pacific when the cycle in convection begins again.

In the west Indian Ocean at about 60°E a small patch of surface convergence and a newly formed positive water vapor anomaly have appeared in a region previously inhabited by dry anomalies. Thus, the preconditioning of the atmosphere in the Indian Ocean has begun and moist anomalies are forming, which are a precursor to a new convective anomaly near 80°E. Strong westerly

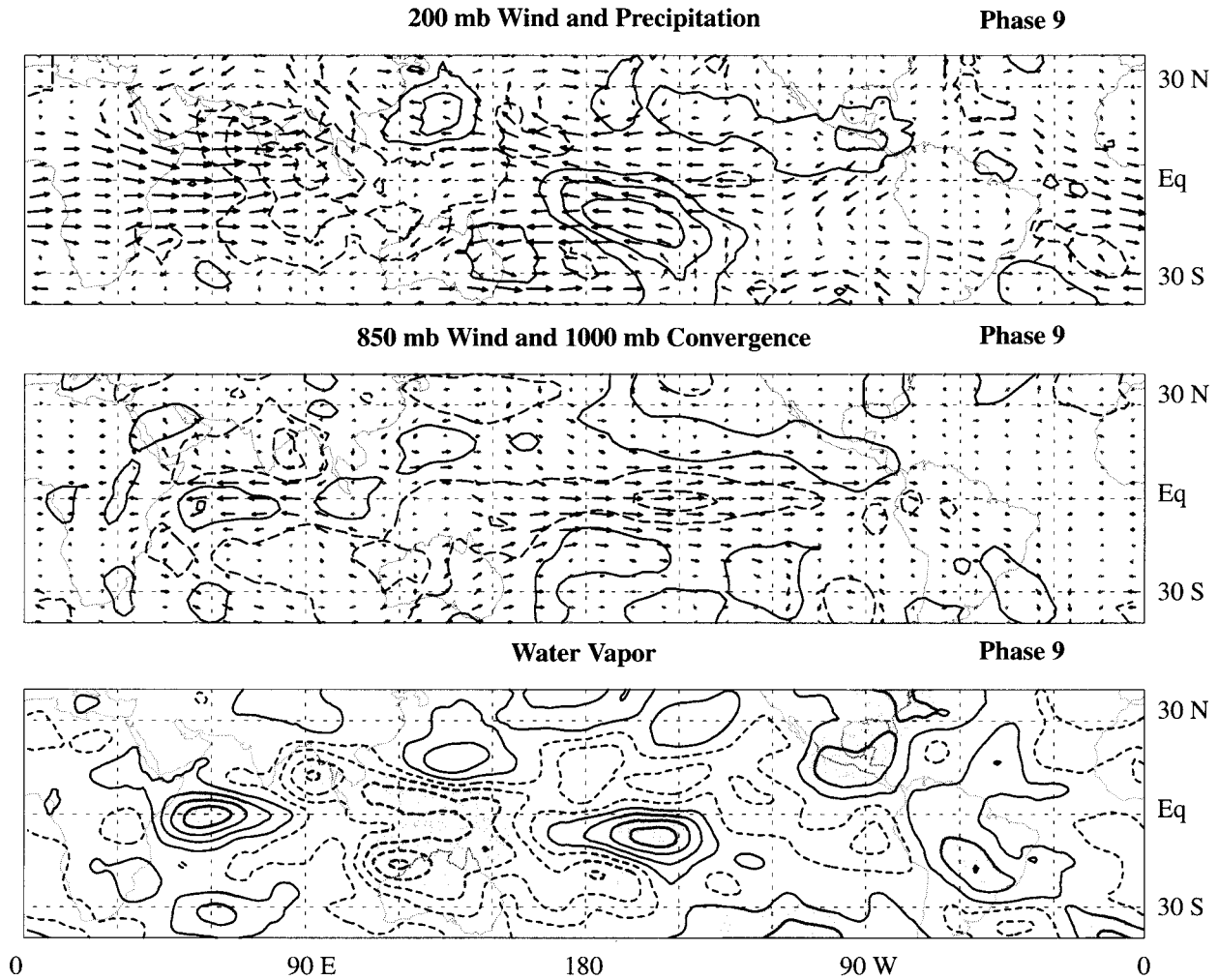


FIG. 14. Same as Fig. 3 but for phase 9.

flow anomalies at 200 mb are expanding into the west Indian Ocean from the west.

#### *i. Phase 9*

If the MJO was periodic, phase 9 would be identical to phase 1. The MJO is not perfectly periodic, but phase 9 (Fig. 14) shows many similarities to phase 1, especially in the water vapor and precipitation fields. The remnants of convection are located to the east of the date line near 10°S, which is reflected in the water vapor and precipitation fields. A strong area of positive water vapor anomalies has grown near 60°E and the equator, which is the precursor to convection in the Indian Ocean mentioned earlier. This feature is being supported by surface convergence and lies within the region of 850-mb easterly wind anomalies. Evidence exists for a weak precipitation anomaly accompanying this water vapor anomaly when the precipitation field is examined for 1988–92 (not shown). A similar anomaly was seen in phase 1.

Enhanced precipitation is occurring along the Mexican and Central American coast as in phase 1, associated with convection there during the Northern Hemisphere summer. Positive moisture anomalies are also found. A tongue of surface divergence and 850-mb westerlies lies along the equator from 120°E to 90°W. Cyclonic flow at 200 mb is beginning to establish itself on either side of the equator at upper levels in the Indian Ocean region.

#### **5. The Northern Hemisphere summer**

Previous studies have noted the seasonal aspects of the MJO, in particular the Indian monsoon during the Northern Hemisphere summer (see Madden and Julian 1994 for a review). Break periods of the monsoon have been attributed in part to different phases of the intra-seasonal oscillation (e.g., Hartmann and Michelsen 1989). Using the index developed in section 3, an enlightening picture of the MJO during Northern Hemisphere summer can be obtained. Composites of 850-mb

**May-October 850 mb Wind and Precipitation Anomalies**

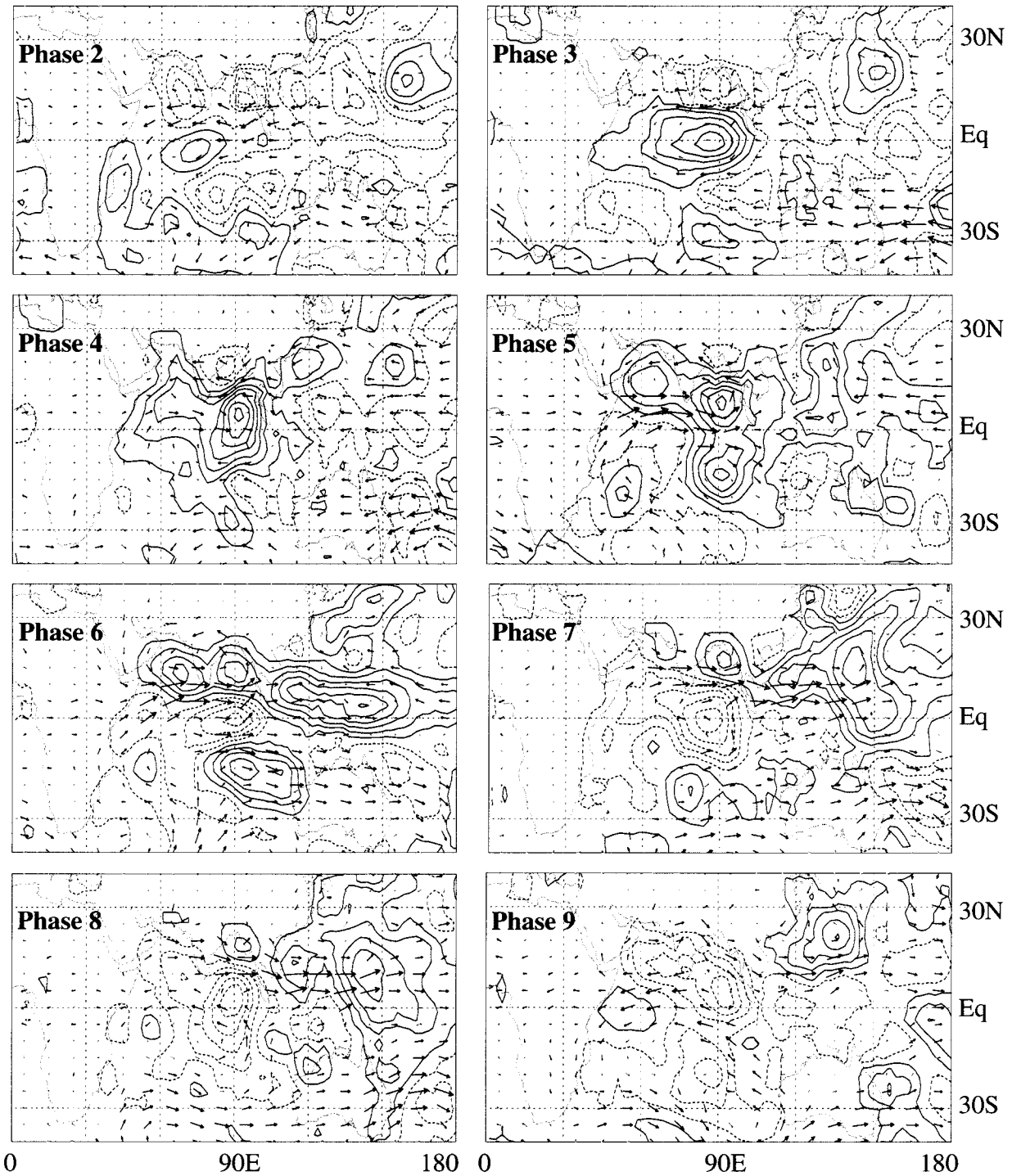


FIG. 15. May-October 850-mb bandpassed wind anomalies and MSU precipitation anomalies as a function of phase for 1979-95. Wind vectors significant at the 90% level are plotted in black and nonsignificant vectors are gray. Contours are every 0.6 mm day<sup>-1</sup> starting at 0.3 mm day<sup>-1</sup>. Maximum vectors are 3.3 m s<sup>-1</sup>. Dashed contours are negative.

wind anomalies and MSU precipitation anomalies for the months May–October in the Indian Ocean region are displayed in Fig. 15. This period encompasses the Indian summer monsoon period and 43 events of the 81 total events derived in the all-season composites fall within this period. Phase 1 is very similar to phase 9 and so only phases 2–9 are displayed in the composite picture. One need only look at phase 9 to see how the cycle of convection is initiated. Since the MSU precipitation dataset is only available over ocean areas, precipitation values over the Indian subcontinent are either nonexistent, or reflective of nearby ocean surfaces through smoothing. However, a very good indication of the widespread precipitation trends over the Indian subcontinent can be inferred by examination of the precipitation fields over the Bay of Bengal and the Arabian Sea to the east and west of the Indian subcontinent. OLR data was used to support inferences about precipitation over the Indian subcontinent, but is not suitable to determine fine spatial structure.

Composites based on the equatorial 850-mb zonal wind index are very similar to those obtained by Hartmann and Michelsen (1989 hereafter referred to as HM) using indices based on precipitation and 850-mb zonal wind for selected observing stations around India. Hartmann and Michelsen (1989) describe active periods of the monsoon as being accompanied by enhanced precipitation centered over central India with an associated cyclonic circulation at 850 mb. Break periods are accompanied by a precipitation minimum over central India with an associated anticyclonic circulation at 850 mb. Spectral analysis indicated that such variations occur on intraseasonal timescales of 40–50 days. These features in the precipitation and winds appear first over the far southern portions of the Indian subcontinent and then propagate toward the north. Precipitation anomalies terminate their northward movement and then die in place once the Himalayas are reached.

The composites in this paper provide a large-scale context for the results of HM. Convection grows along the equator from 80° to 90°E during phases 2 and 3. Westerly wind perturbations at 850 mb begin to knife into the system at phase 4, and the resulting shear spawns a cyclonic circulation to the north of the equator at roughly 10°N with a lesser circulation in the Southern Hemisphere. Precipitation anomalies have reached the southern part of India at this time. At phase 5 the precipitation area near the equator has been completely sheared into two centers to the north and south, consistent with the drying mechanisms discussed in section 4d. Precipitation anomalies have reached central India [confirmed by the OLR signal (not shown)] and are accompanied by a strengthened 850-mb cyclone. This northward and westward propagation of Rossby waves away from the equator explains the northward propagation of the precipitation and wind anomalies seen in HM and other studies. In phase 6, the precipitation maximum and associated cyclonic circulation over central

India are consistent with the active monsoon period described by HM. A dry anomaly is centered over the equatorial Indian Ocean that will propagate northward to eventually provide a break monsoon period for India. Phase 3 is typical of such a period in that a precipitation minimum appears over central India with associated anticyclonic circulation at 850 mb. Phases 7–9 detail the northward propagation of this dry anomaly from the equator. The positive anomaly eventually dies over the north of India (confirmed by the OLR signal).

These composites paint the picture of alternating positive and negative precipitation anomaly areas and associated cyclonic and anticyclonic 850-mb wind circulations beginning in the east equatorial Indian Ocean and then propagating northward and westward across the Indian subcontinent. Weaker precipitation and wind anomaly features occur in the Southern Hemisphere during this season. This pulsation in alternating northward moving wet and dry anomalies is a rather robust feature independent of the portion of the Northern Hemisphere summer record examined and provides compelling evidence in locking at least some of the intraseasonal variability associated with the Indian monsoon to the phases of the MJO. This same type of feature, sometimes described as a northward moving cloud bank when associated with an active monsoon period, has been observed in numerous studies (see Madden and Julian 1994). The timing of the monsoon onset may also be affected by the phase of the MJO, so that the MJO may be important for Indian agriculture (Webster 1987).

## 6. Conclusions

A composite life cycle of the Madden–Julian oscillation based on an 850-mb equatorial averaged zonal wind index has shown that convergence in the boundary layer due to friction plays a key role in the evolution of the Madden–Julian oscillation. The large-scale structure of the MJO is that of a coupled Kelvin–Rossby wave, with wavenumber-1 structure along the equator at upper levels. Equatorial Kelvin wave theory indicates that regions of 850-mb easterlies are accompanied by negative pressure perturbations at the surface and that positive pressure perturbations occur below 850-mb westerlies. Thus, frictional moisture convergence takes place near the surface beneath 850-mb easterly perturbations, and divergence of moisture occurs beneath 850-mb westerly perturbations. The convective complex associated with the MJO generally has moisture convergence in the boundary layer lying along the equator to the east, and divergence to the west. Subsidence or horizontal advection from the west or extratropics associated with Rossby wave circulations may also contribute to drying to the west of convection. Convergence at 850 mb is more bound to the regions of maximum convection (Fig. 7 vs Fig. 8). This phase lag between regions of inviscid convergence and frictional convergence has been noted in other studies (e.g., Hendon and Salby 1994).

Frictional convergence acts to moisten the atmosphere in regions that had been dried out by the previous cycle of convection. A significant correlation exists between surface convergence and positive water vapor anomalies over the west Pacific and Indian Oceans with surface convergence leading water vapor in time (Fig. 6). Convergence at 850 mb has a weaker correlation and lags water vapor over the west Pacific Ocean. The time required for the formation of new convection in a region may be determined by the amount of time it takes surface convergence to reestablish a certain level of moisture. As a prime example, dry anomalies in the west Pacific to the east of the growing area of convection in the Indian Ocean are subjected to a period of moisture convergence (Figs. 4, 5, and 7). The timescale required for convection to shift into the Pacific may be set by the time it takes frictional convergence to sufficiently moisten the atmosphere. Positive water vapor anomalies precede the development of positive precipitation anomalies in areas east of the main convection (Fig. 11). Additionally, water vapor anomalies peak in many areas of the west Pacific before the peak precipitation is detected. A similar process occurs for the onset of convection in the Indian Ocean. Curiously, in the Indian Ocean the main convective area forms to the east of where the initial perturbation in the moisture field is located (Fig. 3 vs Fig. 5).

Rossby wave circulations propagate poleward and westward away from the main convective areas of the Indian and west Pacific Oceans, and accelerate the westerly flow at 850 mb along the equator. This 850-mb westerly flow associated with both the Kelvin and Rossby wave components dries out the equatorial region of the Indian Ocean rapidly, ending convection there. The convection then shifts off the equator with the Rossby components while a second convective center is forming in the west Pacific Ocean. Anticyclonic flow at 200 mb and cyclonic flow at 850 mb are characteristic of these Rossby waves (Figs. 9 and 10). Rossby wave features of the opposite sense can be found in association with dry periods of the oscillation.

During the Northern Hemisphere summer, the Indian monsoon seems intimately tied to phases of the MJO. The northward propagation of precipitation across India during the summer monsoon is associated with northward and westward movement of Rossby wave features trailing the main center of equatorial convection associated with the MJO. Break and active phases of the Indian monsoon seem to be tied to the phases of the MJO. Cyclonic winds at 850 mb accompany active periods, while anticyclonic winds accompany break periods. The composites obtained are consistent with the fields described in Hartmann and Michelsen (1989).

*Acknowledgments.* This work was supported by the Climate Dynamics Program of the National Science Foundation under Grant ATM-9313383.

## REFERENCES

- Bantzer, C. H., and J. M. Wallace, 1996: Intraseasonal variability in tropical mean temperature and precipitation and their relation to the tropical 40–50 day oscillation. *J. Atmos. Sci.*, **53**, 3032–3045.
- Bladé, I., and D. L. Hartmann, 1993: Tropical intraseasonal oscillations in a simple nonlinear model. *J. Atmos. Sci.*, **50**, 2922–2939.
- Gill, A. E., 1980: Some simple solutions for heat-induced tropical circulation. *Quart. J. Roy. Meteor. Soc.*, **106**, 447–462.
- Gruber, A., and A. F. Krueger, 1984: The status of the NOAA outgoing longwave radiation data set. *Bull. Amer. Meteor. Soc.*, **65**, 958–962.
- Hartmann, D. L., and M. L. Michelsen, 1989: Intraseasonal periodicities in Indian rainfall. *J. Atmos. Sci.*, **46**, 2838–2862.
- Hendon, H. H., and B. Liebmann, 1990: The intraseasonal (30–50 day) oscillation of the Australian summer monsoon. *J. Atmos. Sci.*, **47**, 2909–2923.
- , and M. L. Salby, 1994: The life cycle of the Madden–Julian oscillation. *J. Atmos. Sci.*, **51**, 2225–2237.
- Hu, Q., and D. A. Randall, 1994: Low-frequency oscillations in radiative–convective systems. *J. Atmos. Sci.*, **51**, 1089–1099.
- Jones, C., and B. C. Weare, 1996: The role of low-level moisture convergence and ocean latent heat fluxes in the Madden and Julian oscillation: An observational analysis using ISCCP data and ECMWF analyses. *J. Climate*, **9**, 3086–3104.
- Kalnay, E., and Coauthors, 1996: The NCEP/NCAR 40-year reanalysis project. *Bull. Amer. Meteor. Soc.*, **77**, 437–471.
- Knutson, T. R., and K. M. Weickmann, 1987: 30–60 day atmospheric oscillations: Composite life cycles of convection and circulation anomalies. *Mon. Wea. Rev.*, **115**, 1407–1436.
- Lau, K. M., L. Peng, C. H. Sui, and T. Nakazawa, 1989: Dynamics of super cloud clusters, westerly wind bursts, 30–60 day oscillations, and ENSO: A unified view. *J. Meteor. Soc. Japan*, **67**, 205–219.
- Madden, R. A., and P. R. Julian, 1971: Detection of a 40–50 day oscillation in the zonal wind in the tropical Pacific. *J. Atmos. Sci.*, **28**, 702–708.
- , and —, 1972: Description of global scale circulation cells in the tropics with a 40–50 day period. *J. Atmos. Sci.*, **29**, 1109–1123.
- , and —, 1994: Observations of the 40–50-day tropical oscillation—A review. *Mon. Wea. Rev.*, **122**, 814–837.
- Matsumoto, T., 1966: Quasi-geostrophic motions in the equatorial area. *J. Meteor. Soc. Japan*, **44**, 25–42.
- North, G. R., T. L. Bell, R. F. Cahalan, and F. J. Moeng, 1982: Sampling errors in the estimation of empirical orthogonal functions. *Mon. Wea. Rev.*, **110**, 699–706.
- Randel, D. L., T. H. Vonder Haar, M. A. Ringerud, G. L. Stephens, T. J. Greenwald, and C. L. Combs, 1996: A new global water vapor dataset. *Bull. Amer. Meteor. Soc.*, **77**, 1233–1246.
- Salby, M. L., and H. H. Hendon, 1994: Intraseasonal behavior of clouds, temperature, and motion in the Tropics. *J. Atmos. Sci.*, **51**, 2220–2237.
- , R. R. Garcia, and H. H. Hendon, 1994: Planetary-scale circulations in the presence of climatological and wave-induced heating. *J. Atmos. Sci.*, **51**, 2344–2367.
- Seager, R., and S. E. Zebiak, 1994: Convective interaction with dynamics in a linear primitive equation model. *J. Atmos. Sci.*, **51**, 1307–1331.
- Spencer, R. W., 1993: Global ocean precipitation from the MSU during 1979–91 and comparisons to other climatologies. *J. Climate*, **6**, 1301–1326.
- Wang, B., and H. Rui, 1990: Dynamics of the coupled moist Kelvin–Rossby wave on an equatorial  $\beta$ -plane. *J. Atmos. Sci.*, **47**, 397–413.
- , and T. Li., 1994: Convective interaction with boundary-layer dynamics in the development of a tropical intraseasonal system. *J. Atmos. Sci.*, **51**, 1386–1400.
- Webster, P. J., 1987: The elementary monsoon. *Monsoons*, J. S. Fein and P. L. Stephens, Eds., John Wiley and Sons, 3–32.
- Weickmann, K. M., and S. J. S. Khalsa, 1990: The shift of convection from the Indian Ocean to the western Pacific Ocean during a 30–60 day oscillation. *Mon. Wea. Rev.*, **118**, 964–978.